Fuel 361 (2024) 130613

Contents lists available at ScienceDirect

Fuel

journal homepage: www.elsevier.com/locate/fuel

Full length article

Investigation of the effect of hydrogen addition on soot and PAH formation in ethylene inverse diffusion flames by combined LII and PAH LIF

Chinonso Ezenwajiaku [a,*], Robert Roy [b], Midhat Talibi [a], Ramanarayanan Balachandran [a], Iain S. Burns [b]

[a] Department of Mechanical Engineering, University College London, London, WC1E 7JE, UK
[b] Department of Chemical and Process Engineering, University of Strathclyde, Montrose Street, Glasgow, G1 1XJ, Scotland, UK

ARTICLE INFO

Keywords:
Inverse diffusion flame
Hydrogen
Laser-induced incandescence (LII)
Soot
Polycyclic aromatic hydrocarbons (PAH)
Planar laser-induced fluorescence (PLIF)

ABSTRACT

It is shown that signals from both laser-induced incandescence (LII) of soot and laser-induced fluorescence (LIF) of polycyclic aromatic hydrocarbons (PAHs) decrease with hydrogen addition (in volume fractions of 3%, 6% and 9% with respect to the fuel mixture) to ethylene–air inverse diffusion flames (IDFs). The structure of the IDF suppresses soot oxidation and the effect of hydrogen addition under these conditions has been studied. Experiments were performed using a frequency-doubled, pulsed dye laser to perform planar LIF of PAH, and a pulsed fibre laser to perform LII. In relative terms, the LII signal decreases more sharply than the PAH LIF signal. This would be consistent with the dependence of soot inception on PAH concentration as well as the suppression of soot growth via the reduced concentration of PAH and perhaps other precursors such as acetylene. Similar trends in relative signal decrease are observed at a range of heights above the burner, despite the measurement locations encompassing a wide range of absolute signal levels. As a comparison, the influence of adding methane to the IDF in the same volume fractions was also studied and found to suppress PAH LIF and LII signals but to a far lesser extent than in the case of hydrogen.

1. Introduction

Despite the drive for alternative sources of energy for modern combustion systems, hydrocarbon fuels remain dominant. These fuels produce emissions which are hazardous to human health and have adverse effects on the global climate [1]. A proportion of these effects is attributed to soot particulates which have been shown to contribute significantly to global deaths related to cardiovascular and pulmonary diseases from air pollution [1]. Studies have shown that prolonged exposure to soot particles can cause cancer primarily due to polycyclic aromatic hydrocarbons (PAHs) which are building blocks of soot and are adsorbed on the surface of exhaust soot particles [2]. Furthermore, formation of soot negatively affects the performance of combustors in engines and gas turbines and thus reduces their lifetimes [3]. The accurate measurement of PAHs and soot is key to understanding their complex formation processes and hence reducing their formation in combustion systems. Numerical models can be deployed to study soot formation processes in flames and combustors, but these numerical studies need accurate experimental data for validation of the models. Therefore, careful and relevant experimental studies remain a necessity both to progress the understanding of soot formation and to improve the predictive capability of numerical models.

To understand the complex processes involved in formation of PAH and soot, various open flame configurations have been used including premixed and non-premixed flames [4–9]. Non-premixed (or 'diffusion') flames have been shown to be particularly suitable to track the early stages of PAH formation and understand fuel molecular structure effects on soot formation [10]. In this regard, the inverse diffusion flame (IDF) provides good separation between the pyrolysis and oxidative processes and as a result, produces a relatively larger amount of PAH and soot compared to the normal diffusion flame (NDF). In the IDF configuration, the oxidiser is supplied through the central tube and the fuel is passed through an inner annular ring, while an outer co-annular flow of inert gas shields the flame from ambient air. As a result, the combustion products are formed, and convected away, on the fuel-rich side of the reaction zone, hence obviating significant oxidation of soot [5,8,11]. Ethylene fuel has been used for much of the previous research on soot formation [12–15] due to its high sooting propensity and significant concentration as an intermediate species in the decomposition of most large hydrocarbon fuels [12,13].

Laser-Induced Incandescence (LII) is a commonly utilised non-intrusive optical diagnostic technique for the study of soot formation [16] and is applied both to flames of conventional hydrocarbons

* Corresponding author.
E-mail address: chinonso.ezenwajiaku@ucl.ac.uk (C. Ezenwajiaku).

https://doi.org/10.1016/j.fuel.2023.130613
Received 4 August 2023; Received in revised form 30 October 2023; Accepted 11 December 2023
Available online 21 December 2023

and of biofuels [17–23]. Conventionally, it involves the use of the fundamental beam from a pulsed Nd:YAG laser at 1064 nm or frequency doubled beam at 532 nm to heat up the soot particles to temperatures of approximately 4000 K to emit incandescence [24–27]. The infrared laser excitation is preferred to avoid interference from laser-induced fluorescence (LIF) of polycyclic aromatic hydrocarbons (PAHs) or incipient structures [16,28,29]. The use of fibre lasers for LII has been investigated previously due to the potential advantages of safe and efficient beam delivery to industrial test environments [30]. Pulsed fibre lasers have been shown as viable alternative excitation source for LII because they can generate moderately high-energy pulses at a high pulse repetition rate and with good beam quality. Fibre lasers of this type are also rugged and fairly compact, thus allowing them to form part of a transportable measurement system [31,32]. Initial studies using pulsed fibre lasers to demonstrate LII have focused on measuring soot particle distribution at the exhaust plumes of small-scale aero-engines [30–32]. More recently, a systematic study of the application of LII with pulsed fibre lasers was performed in laminar flat flames, complemented by modelling of LII signal generation in response to the longer pulse duration that is a feature of fibre lasers [33]. It was shown that relative measurements of soot volume fraction (SVF) can be performed in laminar flames, in 1D line-imaging mode. The same pulsed fibre laser source has also been used for in-situ photo-acoustic measurements of soot distribution in a premixed C_2H_4-air flat flame [4].

To reduce the formation of soot in hydrocarbon flames, researchers have explored the addition of hydrogen to the primary fuel [12,34–36]. Xu et al. [37], for example, studied the effect of H_2 addition on soot formation in counterflow diffusion flames of CH_4 and C_2H_4 using planar LII. The authors isolated the chemical effects of H_2 on soot formation in the mixture by studying reference flame conditions using He addition. They reported higher soot reduction for H_2 than He doped flames for both C_2H_4 and CH_4 primary fuel. The reduction of SVF by H_2 addition for both primary fuels was attributed to the suppression of PAH growth and soot inception processes. Gu et al. [36] numerically studied the effect of adding H_2 and CO_2 to a C_2H_4 co-flow normal diffusion flame on soot formation and observed that both additives reduced SVF. They concluded that H_2 was more effective in suppressing soot inception processes by reducing PAH concentrations while CO_2 suppressed HACA (H-abstraction-C_2H_2 addition) based soot surface growth processes by lowering the temperature and H-abstraction rates. De Iuliis et al. [38] investigated the effect of adding up to 40% H_2 to rich C_2H_4/air premixed flames (with constant C/O ratio of 0.77) using laser scattering/extinction techniques and transmission electron microscopy (TEM) for SVF and soot morphology parameters (volume-mean diameter, primary particle diameter and radius of gyration). Their results showed reduction in SVF, volume-mean diameter and primary particle diameter, with no significant changes in flame temperature profile. The authors attributed this to reduced H-abstraction rates which caused a reduction in PAH formation.

Another additive which has been investigated for its effect on soot formation in various binary fuel mixtures is CH_4 [17,39,40]. Roesler et al. [40] investigated the effect of CH_4 addition to C_2H_4 co-flow normal diffusion flame on PAH and soot formation using electron-impact/quadrupole mass spectrometry and photo-ionisation/time of flight mass spectrometry for PAH, and LII for SVF. The authors observed that when the adiabatic flame temperature of the mixtures is kept constant, the SVF and PAH concentration increased with increase in the volume of CH_4 in the fuel mixture. This enhancement in PAH concentration and SVF was attributed to the production (via pyrolysis of CH_4) of methyl radicals which promote the formation of PAH through the propargyl recombination reaction. Hwang et al. [41] studied soot formation in co-flow normal diffusion flames for binary fuel mixtures of C_2H_4 and CH_4 using light extinction and LIF for SVF and PAH respectively. Contrary to observations by Roesler et al. [40], they reported that the SVF decreased linearly with increase in the proportion of CH_4 in the fuel mixture, which they attributed to the reduction in the concentration of C_2H_2 as a result of CH_4 addition. However, they observed a slight increase in PAH concentration with increase in CH_4 which they too suggested could possibly be due to the propargyl recombination reaction. Ni et al. [42] investigated the effects of adding CH_4 to a C_2H_4 laminar normal diffusion flame on soot formation using LII and LIF for soot and PAH respectively. They observed a reduction in both PAH LIF and LII signals as the volume of CH_4 was increased in the fuel mixture. Trottier et al. [17] also studied soot formation in various binary fuel mixtures including CH_4 and C_2H_4 experimentally and numerically. They argued that the enhancement of soot formation with increase in the volume of CH_4 present in the binary mixture of CH_4/C_2H_4 was temperature dependent. These conflicting observations from various studies of CH_4/C_2H_4 binary fuel mixtures as outlined above require further investigation.

More systematic experimental work is needed to better understand soot formation processes in binary mixtures of C_2H_4 and H_2. Studying the relationship between PAH and soot in the IDF where soot formation can be separated from oxidation provides a useful test-case but thus far has received little attention in the context of H_2 addition. We present a comprehensive experimental investigation of the effect of hydrogen addition on an ethylene IDF based on multi-parameter laser imaging. The effect of methane addition to the ethylene flame is also studied. Laser-induced incandescence is demonstrated using a long-pulsed fibre laser and combined with simultaneous OH LIF imaging. Simultaneous LIF imaging of PAH and OH is also performed with the aim of understanding the relationship between the soot and PAH formed in the binary fuel mixtures investigated.

Table 1
The flow conditions of the flames tested in this study.

Set	PF	SF	Q_{PF} (slpm)	Q_{SF} (slpm)	X_{SF} (%)	C to H ratio
A	C_2H_4	H_2	6	0	0	0.50
				0.2	3	0.49
				0.4	6	0.48
				0.6	9	0.48
B	C_2H_4	CH_4	6	0	0	0.50
				0.2	3	0.49
				0.4	6	0.48
				0.6	9	0.48

Where PF — primary fuel; SF — secondary fuel; Q_{PF} — volumetric flow rate of the primary fuel; Q_{SF} — volumetric flow rate of the secondary fuel; X_{SF} — volume fraction of the secondary fuel in the binary mixture. The standard temperature and pressure at which volumetric flow rates are quoted are 25 °C and 1 bar respectively.

2. Methodology

Diffusion flames were stabilised on an IDF burner, which has been described previously [43], hence only a brief description is presented here. It consists of three concentric stainless-steel tubes with inner diameters of 10, 30 and 64 mm with the tube lips finished to a knife-edge to reduce the effect of rim thickness. Flow conditioning was achieved with steel balls of diameters 3 mm and 5 mm in the co-flow passages. Fuel gases were passed through the central tube, while air was passed in the first co-annular tube. To shroud the flame and reduce air entrainment, N_2 was passed through the second (outer) co-annular tube.

Table 1 summarises the flow conditions in this study. The flow rates of primary fuel, C_2H_4, and air were fixed at 6 slpm and 1.2 slpm respectively throughout the study. Varying volumes of secondary fuels H_2 and CH_4 were separately added to the primary fuel from 0 to 9% as shown in Table 1 to study their effects on sooting tendency. The volume fraction of the secondary fuel is defined as follows:

$$X_{SF} = \frac{Q_{SF}}{(Q_{SF} + Q_{C_2H_4})} \quad (1)$$

where Q_{SF} and $Q_{C_2H_4}$ represent the volumetric flow rates of the secondary fuel (H_2 or CH_4) and of C_2H_4 respectively. To ensure that the addition of SF did not have a considerable impact on the global flame behaviour, the C/H ratio of the binary mixtures tested was kept within a narrow range of 0.49 ± 0.01 (See Table 1). Additionally, the OH PLIF images captured for the different test conditions did not show any significant changes in several aspects of the global flame behaviour (flame height, peak OH signal, and OH profile width). Radial OH LIF line profiles for the base case and maximum H_2 and CH_4 conditions are presented in Fig. 2(e).

For each flow condition shown in Table 1, LII and OH LIF images were captured simultaneously, followed by separate simultaneous imaging of PAH LIF and OH LIF. For each test condition, 200 instantaneous images were acquired. Fig. 1 shows a schematic of the experimental setup, including the cameras and optical arrangements. The simultaneous imaging schemes are discussed in more detail in the subsequent sections.

2.1. Simultaneous PAH and OH LIF imaging

The second harmonic output from an Nd: YAG laser (Litron Nano-PIV) was used to pump a tuneable dye laser (Fine Adjustments Pulsare-S model) with Rhodamine 6G dye. The frequency-doubled output from the dye laser was tuned to near 283 nm to coincide with the Q1(5) transition of the $A^2\Sigma^+ \longleftarrow X^2\Pi(1,0)$ band for the excitation of the OH radical. The beam was converted to a light sheet of height 50 mm and thickness 0.15 mm (at the focus) using cylindrical lens (f = −40 mm) and spherical bi-convex lens (f = 500 mm). The same laser was utilised to excite PAH species. Simultaneous detection of OH and PAH was achieved with two intensified charge coupled devices (ICCDs) placed on either side of the IDF burner and at right angle to the plane of the laser sheet. The ICCDs consist of a Videoscope intensifier (VS4-1845) coupled to a PCO Sensicam CCD camera system. The OH fluorescence was filtered near 310 nm using ICCD-1 fitted with a UV 100 mm f/2.8 Cerco lens and a combination of WG 305 and UG11 Schott glass filters. ICCD-2, fitted with an f/1.2 Nikon lens of focal length of 50 mm and a combination of BG12 and GG420 Schott glass filters, was used to detect fluorescence from PAH species of three or more rings between 420 nm and 480 nm [44,45]. The reasons for the PAH detection regime chosen and the suitability of the LIF technique for analysing PAHs have been discussed in detail in our previous study [43]. The camera gating for PAH detection was set at 80 ns. Also, it is important to note that the quantitative measurement of PAHs is non-trivial. This is due to the difficulty in distinguishing the spectral properties between PAH molecules with the same number of rings but different chemical structures because of the characteristic broadband emission spectra from these PAHs [46,47]. The possibility of detecting LIF from PAH dimers cannot be discounted [48], although these may be expected to be more prevalent further downstream. Hence, only qualitative trends for PAHs are provided in this study.

2.2. Simultaneous LII and OH PLIF imaging

The same set-up as described above was employed for the OH excitation and detection. Long-pulse LII excitation was achieved with a commercially available 1060 nm wavelength fibre laser (SPI redEnergy G4 20 W EP-Z). The divergent output beam from the fibre laser was focussed using a spherical lens of 400 mm focal length. The pulse repetition rate was 10 kHz and the pulse duration was roughly 200 ns. The laser pulse energy was determined using a thermopile power meter. The fibre laser output power is adjustable by varying the drive current of the pump diode laser: a pulse energy of 0.7 mJ was used throughout. To avoid significant variation in beam diameter over the thickness of the soot sheet, the laser was focussed about 10 mm in front of the region of interest. This resulted in a fluence (defined based on the $1/e^2$ beam diameter of roughly 650 μm) of approximately 210 mJ cm^{-2} at the measurement location.

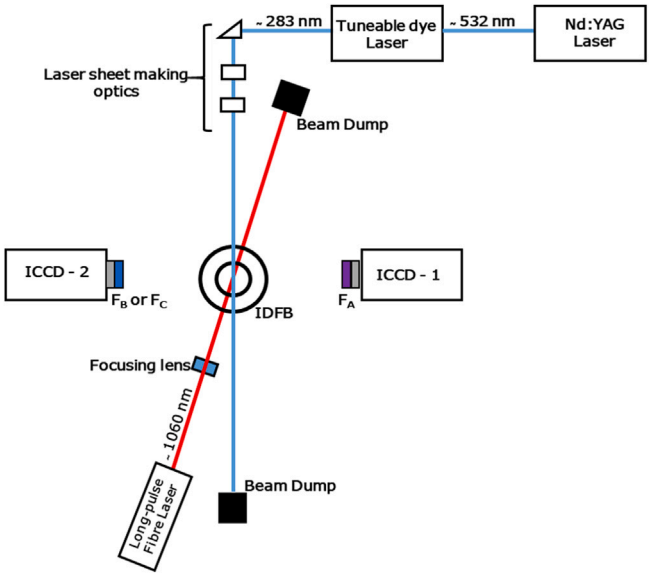

Fig. 1. Schematic of the experimental arrangement used for simultaneous LII and OH PLIF imaging and separate simultaneous PLIF imaging of PAH and OH. The angled layout of the fibre laser is exaggerated for clarity. ICCD — Intensified charge coupled device, IDFB — Inverse diffusion flame burner, F_A — Filter A (UG11 + WG 305), F_B — Filter B (BG12 + GG 420), F_C — Filter C (450 nm bandpass filter with FWHM of 10 nm).

Detection of LII was achieved with ICCD-2 fitted with an f/1.2 Nikon lens of focal length of 50 mm and a bandpass filter centred at 450 nm (FWHM = 10 nm), chosen to avoid interference by emission from C_2 and C_3 radicals. The camera gating for LII detection was set at 210 ns to include the laser pulse duration. The angled layout of the fibre laser in Fig. 1 is exaggerated for clarity. The laser beam from the fibre laser was angled only slightly (roughly 5°) with respect to the PLIF excitation beam to retain an orientation near perpendicular with the ICCD-2 collection axis. The fibre laser was used as the master signal to the synchroniser controlling the triggering of the Nd:YAG laser pumping the dye laser, as well as triggering the cameras for simultaneous OH LIF and LII detection. The fibre-laser LII generates 1D line images of soot in the flame. The LII signals provide a relative measure of soot volume fraction, which is sufficient to reveal the influence of fuel composition and to compare with the changes in PAH LIF under the same sets of conditions.

For the flames with H_2 addition (set A in Table 1), measurements were performed with the fibre-laser beam displaced to three different heights above burner (HAB), 6 mm, 8 mm and 10 mm, each time capturing LII and OH PLIF simultaneously. This was done to confirm whether the effect of H_2 on soot and PAH might vary with location in the flame. For the flames with CH_4 addition (set B in Table 1), LII and simultaneous OH PLIF imaging measurements were performed at 10 mm HAB only, to compare the effect of an alternative additive.

2.3. Image analysis

Fig. 2 shows examples of overlayed PAH LIF, LII and OH LIF images. PAH LIF and LII signals were each separately imaged with OH LIF simultaneously. The OH LIF images allow the locations of the soot and PAH LIF to be referenced with respect to the position of the flame front. The OH LIF profiles also serve as a check that the flame was stable, with the reaction zone location maintained between data sets. Fig. 2(a) and (b) show the LII signal together with the OH LIF signal and PAH LIF signal together with the OH LIF signal respectively. Data

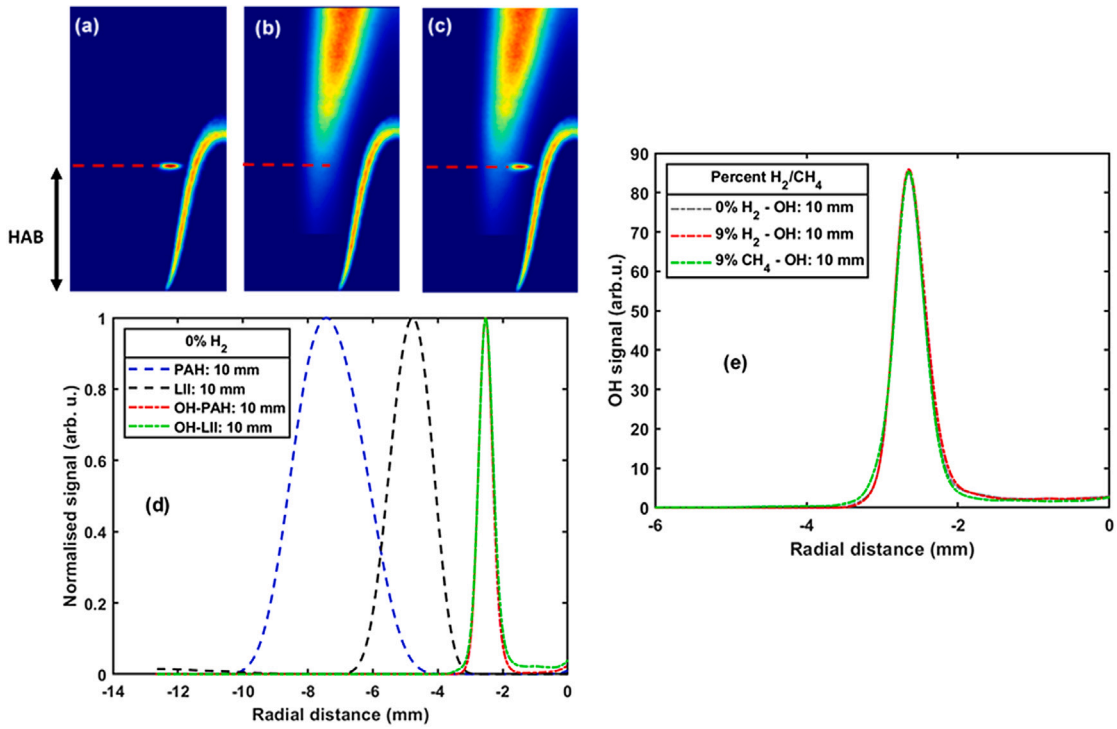

Fig. 2. (a) LII and OH LIF combined image (b) PAH LIF and OH LIF combined image (c) OH LIF, LII and PAH LIF combined image (d) The combined OH LIF, LII and PAH LIF line profile at HAB of 10 mm (centred using the OH line profile). (e) OH LIF line profiles at HAB of 10 mm for 0% and 9% H_2 and CH_4 addition. Note: OH-PAH and OH-LII refer to the OH LIF radial profiles obtained from simultaneous OH/PAH LIF and OH LIF/LII respectively.

processing involved averaging the 200 acquired images and subtracting the background. The images were scaled to coordinates of HAB and radial distance from the burner centre line using reference images of a ruler sitting above the burner within the excitation plane. The scaled images are combined and shown in Fig. 2(a)–(c), which is for the flame without secondary fuel addition. Soot is present at an intermediate location, between the reaction zone and the broader zone where PAH LIF is observed. Note that 1D line imaging of soot was performed, in this case at 10 mm HAB. The images shown in Fig. 2(a)–(c) are from the point of view of camera 2, i.e. a mirror image of the OH LIF data from camera 1 is shown. Thus, these images relate to the side of the IDF closer to the dye laser source in Fig. 1. All subsequent analysis has been performed on the image data for this half of the axisymmetric flame. The representative line profiles obtained from Fig. 2(c) at HAB of 10 mm, indicated by a red line, are presented in Fig. 2(d) for the same flame conditions. Radial OH LIF line profiles for the base case and maximum H_2 and CH_4 conditions are presented in Fig. 2(e). It is important to reiterate here that the radial OH LIF line profiles shown in Fig. 2(e) indicate no significant changes in several aspects of the global flame behaviour for the different conditions tested. Subsequent sections present data evaluated based on the radial maxima of the PAH LIF and LII signals at three heights above the burner and for a range of flame conditions. Additionally, to provide an idea of the spread of LII and PAH at each height investigated, the widths of the LII and PAH were obtained using the full-width at half-maximums (FWHMs) of their respective line profiles. The area under the curve of the radial profile for LII and PAH was also estimated as a measure of the total magnitude of signals at each HAB. The estimated profile widths and the area under the curve will be referred to as FWHM and area respectively in the subsequent sections of this paper.

3. Results and discussion

In this section, the effects of H_2 and CH_4 addition on PAH LIF and LII signal levels at a range of HABs are presented. The relative changes in PAH LIF and LII signals with increasing amounts of secondary fuel are then compared to establish if a correlation exists between these effects.

3.1. Effect of H_2 addition

Fig. 3 shows the radial peak values for PAH LIF and LII for various levels of H_2 addition presented as a function of HAB. It can be seen that at each H_2 addition, the peak signals for both PAH and LII increased monotonically as HAB increased from 6 mm to 10 mm. This could be attributed to the effects of increased residence time due to increased HAB leading to increased formation and growth of both PAH and soot [49]. It is worth noting that PAH LIF signal increases by a factor of about 2.9 and LII signal by a factor of about 4.3 between 6 mm and 10 mm HAB for the undoped flame.

Fig. 4 shows the radial line profiles for PAH LIF and LII at various heights (a), and with and without H_2 addition (b). These radial profiles highlight that the shapes and locations of the signal profiles change little with HAB or with addition of H_2. For the purpose of comparison, the LIF and LII signals have been normalised through division by the respective signal maxima for the additive-free flame. In Fig. 4(a), the radial line profiles for PAH and LII are presented for 0% H_2 addition at three different HABs: 6 mm, 8 mm and 10 mm. It can be seen that for both PAH and LII, as the HAB increased from 6 mm to 10 mm, the peak location shifted very slightly (by about 0.3 mm) inwards towards the centre of the burner (indicated as the zero position on the plot). A similar shift in peak PAH LIF location was observed by Mikofski et al. [11] which was attributed to cold fuel entrainment of the buoyant flame plume. Also, the profile widths increased very slightly with height, which could be attributed to the formation of more soot and PAH as the HAB increases (see Fig. 3). This is consistent with the shape of the PAH LIF profile shown in Fig. 2(b), where the PAH-containing zone becomes broader and shifts closer to the burner centre-line with increasing HAB. In Fig. 4(b), the radial profiles for PAH and LII with 0% and 9% H_2 addition at HAB of 10 mm are presented. It can be seen that as H_2 addition levels increased from 0% to 9%, the peak values for both PAH LIF and LII decreased by 37% and 63% respectively. The reduction in the peak signals for PAH and LII with H_2 addition could be due to the effect of H_2 addition on the reversible

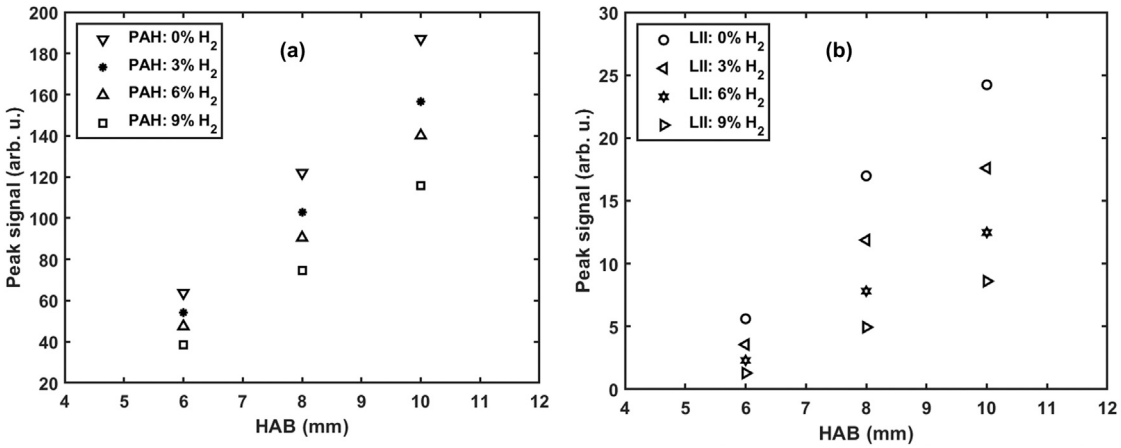

Fig. 3. (a) Peak PAH signal expressed as a function of HAB for various H_2 addition (b) Peak LII signal expressed as a function of HAB for various H_2 addition.

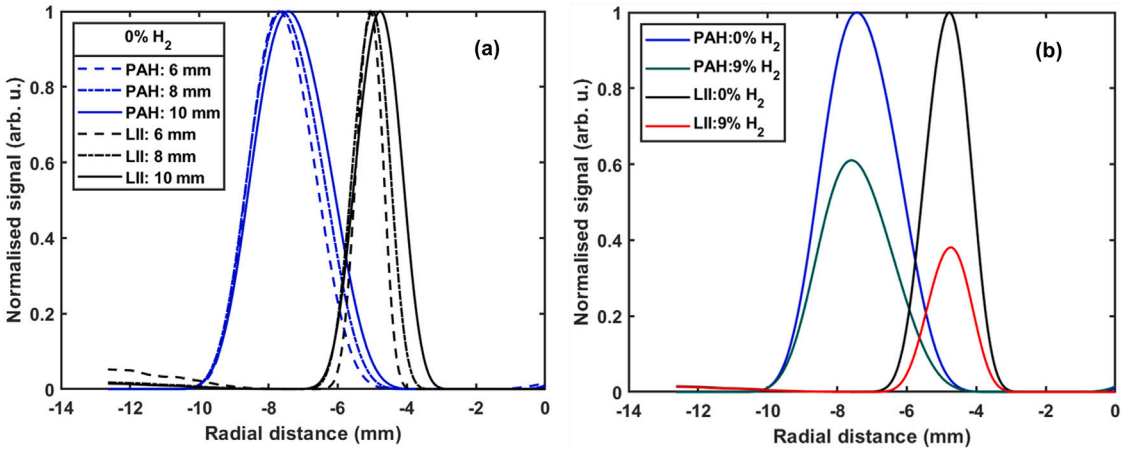

Fig. 4. (a) Normalised radial line profiles of PAH and LII signals at three different heights above the burner (HAB): 6 mm, 8 mm and 10 mm for 0% H_2 addition. The line profiles were normalised with the respective peak values for each height. (b) Normalised radial line profiles of PAH and LII at HAB of 10 mm for 0% and 9% H_2 addition. The profiles were normalised with the peak value for 0% H_2 addition.

reaction ($A_i + H \rightleftharpoons A_{i-} + H_2$) for PAH growth through the HACA route [50,51], where A_i is an aromatic molecule consisting of i aromatic rings and A_{i-} is a corresponding aromatic radical. Increasing the level of H_2 reverses the H-abstraction reaction of the HACA mechanism which inhibits the availability of the aromatic radical (A_{i-}) for further mass addition reactions and hence reduces the abundance of larger PAH molecules available for soot inception and growth.

To understand the effect of H_2 addition on the total magnitude of PAH LIF and LII signals, the areas under the curves for the radial profiles of PAH LIF and LII at HABs of 6 mm, 8 mm and 10 mm are presented in Fig. 5(a). The widths of the radial profiles for PAH and LII, estimated based on the full-width-at-half-maximum (FWHM), are presented in Fig. 5(b). Fig. 5(c) shows the variation in the radial peak PAH LIF and LII signals with H_2 addition. It can be seen that at all heights presented, the addition of H_2 reduced the signal level far more significantly than the FWHM for both PAH LIF and LII. In Fig. 5(b), little reduction (<10%) in the widths of PAH LIF and LII profiles with increasing H_2 addition is clearly evident, except for the case of the LII signal at 6 mm HAB (~18% decrease). Accordingly, the plots for integrated areas and radial peak signals show very similar behaviour. Hence, either the peak signal or area under the curve plots could be used to represent trends for PAH and LII analysis. From Fig. 5(a) and (c), it can be seen that as the level of H_2 addition increased, the fractional reduction in the PAH LIF signal was near-identical at all heights investigated. For LII, similar trends are observed at each HAB, although the signal showed slightly more pronounced reduction at lower positions (a reduction in peak LII signal by up to ~ 77% was observed at 6 mm HAB compared to a ~ 63% drop at 10 mm). A similar trend was observed by Wang et al. [52] in their study of hydrogen-enriched C_2H_4 normal diffusion flames.

Comparing PAH LIF and LII, the normalised signals reduced more sharply with H_2 addition for LII than for PAH LIF at all heights studied. At each H_2 addition level, the fractional reduction in the peak LII signal was found to be approximately 1.5 times greater than for the peak PAH LIF signal. This general trend may be consistent with expectations, given the pivotal role of PAH molecules both in the inception and growth of soot. The dimerisation of larger PAH molecules is considered to be a crucial step in soot inception and its rate depends non-linearly on PAH abundance [48,49]. Likewise, H_2 addition also influences the growth rate of soot particles. It has been shown that two processes are important for soot growth in diffusion flames, the HACA mechanism and PAH adsorption [49,53]. The addition of H_2 is therefore likely to influence the growth rate of soot not only through its impact on concentration of 3–4 ring PAH molecules but also by influencing the concentrations of other species involved in soot growth, such as acetylene [54].

3.2. Effect of CH_4 addition

In this section, the effects of CH_4 addition on PAH LIF and LII are discussed. Fig. 6 shows the PAH LIF and LII radial line profiles obtained at HAB of 10 mm for 0% and 9% CH_4 addition. Similar to the

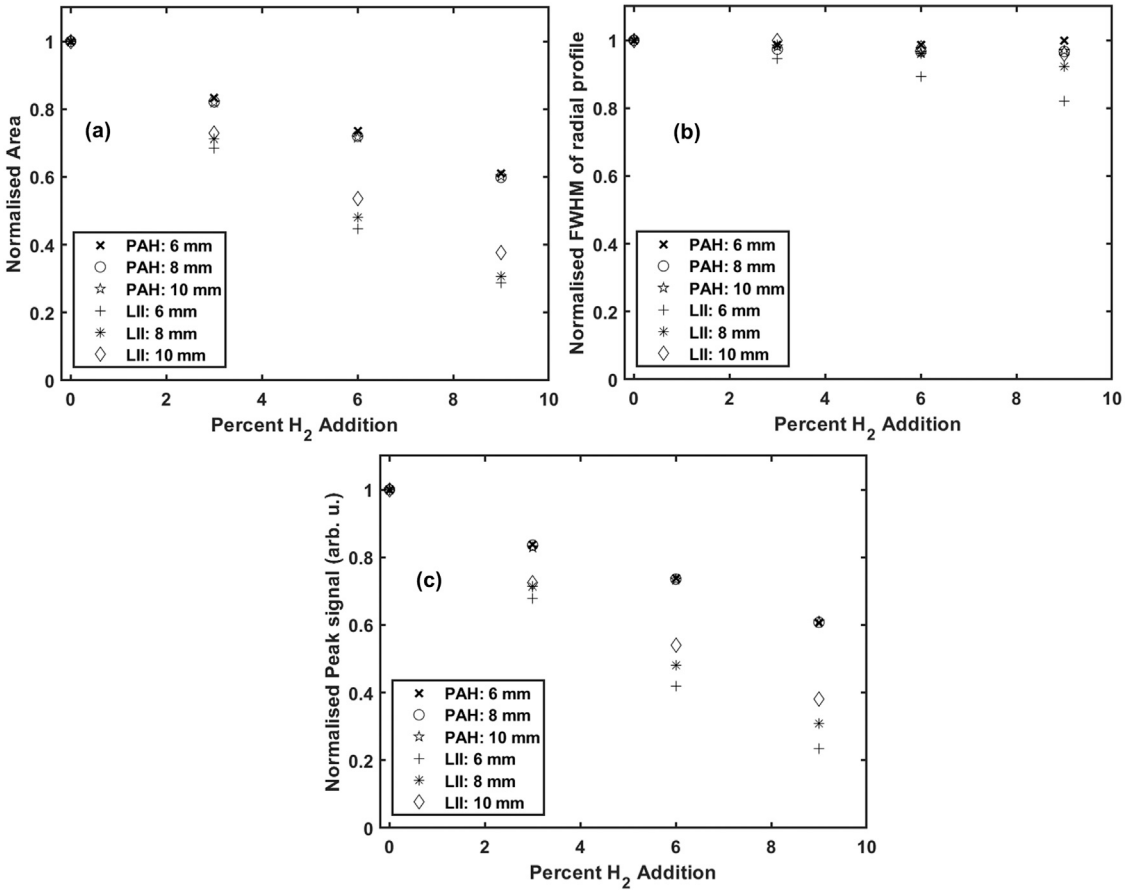

Fig. 5. (a) The area under the curve, (b) the profile width (FWHM) and (c) the peak signal, of the radial profiles for PAH LIF and LII, normalised with the peak values for PAH LIF and LII presented as a function of H_2 addition (% v/v) at three different heights above the burner (HAB): 6 mm, 8 mm and 10 mm.

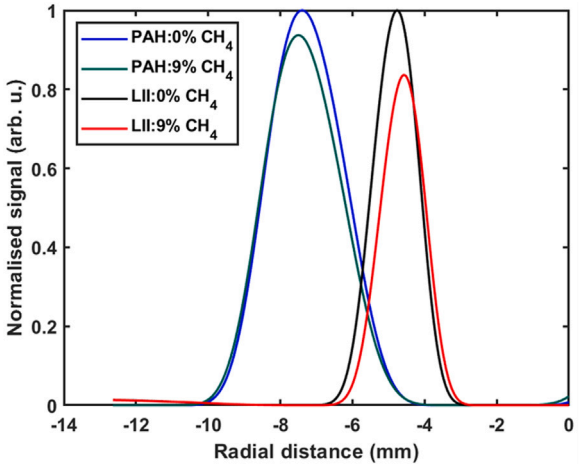

Fig. 6. Normalised radial line profiles of PAH and LII at HAB of 10 mm for 0% and 9% CH_4 addition. The profiles were normalised with the peak value for 0% CH_4 addition.

observations in the H_2 addition case (see Fig. 4(b)), it can be observed that as the CH_4 level is increased from 0% to 9%, the profile width and the peak values decreased for both PAH LIF and LII, although here the reduction in signal levels is far more modest. Again, to understand the effect of CH_4 addition, the radial integral of PAH LIF and LII signals, the FWHM of the radial profiles, and the radial peak signal levels are presented in Fig. 7. PAH LIF data are presented for HAB of 6 mm, 8 mm and 10 mm while LII values are presented at only 10 mm.

From Fig. 7(a) and (c), it can be seen that as CH_4 level increased, signal levels are reduced at all heights presented for both PAH LIF and LII. As in the case of H_2 addition, the integral area and peak height plots show very similar trends. It can be observed that LII signals showed a proportionally greater reduction when compared with the PAH LIF signals. It should be noted that the effect of CH_4 addition is far less pronounced than the addition of an equivalent volume fraction of H_2: note the expanded vertical scale for the plots concerning CH_4. In Fig. 7(b), it can be observed that CH_4 does not make a significant difference to the widths of the PAH LIF profiles and any effect on the width of the LII radial profile at 10 mm HAB is slight.

It is worth noting in Fig. 7(a) and (c) that at HAB of 10 mm, the LII signals showed a higher fractional reduction than PAH LIF signals at all levels of CH_4 addition. This shows that a reduction in PAH levels is associated with a larger fractional reduction in LII irrespective of whether H_2 or CH_4 is used as the additive. The explanations for this may be similar to those discussed above in relation to H_2 addition. Another interesting feature of the results for CH_4 addition is that the relative effect on PAH LIF signals is greater at lower HAB, in contrast to H_2 addition for which the relative change in LIF signal was near-identical at each HAB.

To compare the effects of H_2 and CH_4 addition to the C_2H_4 IDF on PAH LIF and LII, the normalised peak LII signal is presented as a function of normalised peak PAH signal in Fig. 8. The data for H_2 addition include all three heights studied: 6 mm, 8 mm and 10 mm. It can be seen from Fig. 8 that the magnitude of reduction in the peak signals for both PAH LIF and LII were significantly higher with H_2 addition when compared to CH_4 addition. For example, with 9% H_2 addition, PAH LIF and LII showed reductions of about 40% and 70% respectively, as compared to about 7% and 17% reductions PAH

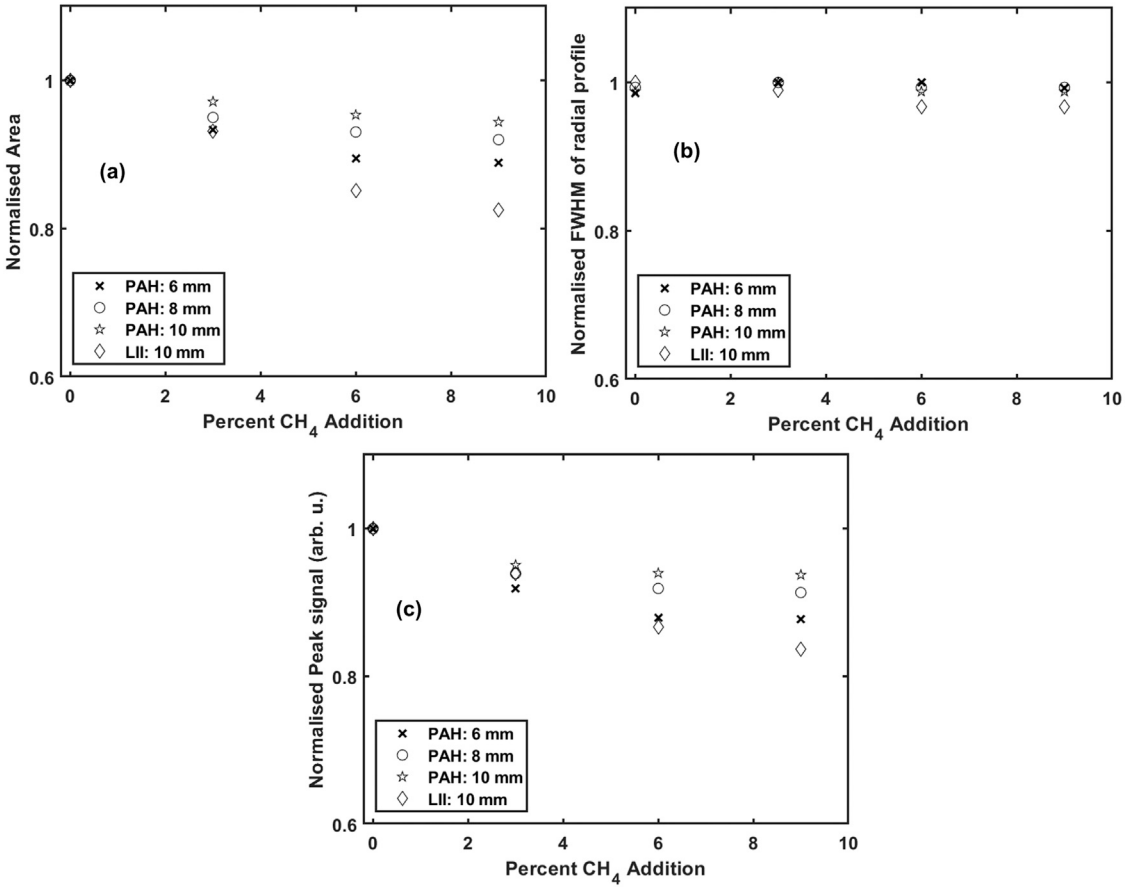

Fig. 7. (a) The area under the curve (b) the profile width (FWHM) of the radial profiles for PAH LIF and LII normalised with the peak values for PAH LIF at HAB of 6 mm, 8 mm and 10 mm and LII at HAB of 10 mm presented as a function of CH_4 addition (% v/v) and (c) Normalised peak signals for PAH and LII presented as a function of percent CH_4 addition (% v/v) at HAB of 6 mm, 8 mm, and 10 mm (for PAH) and at HAB 10 mm for LII.

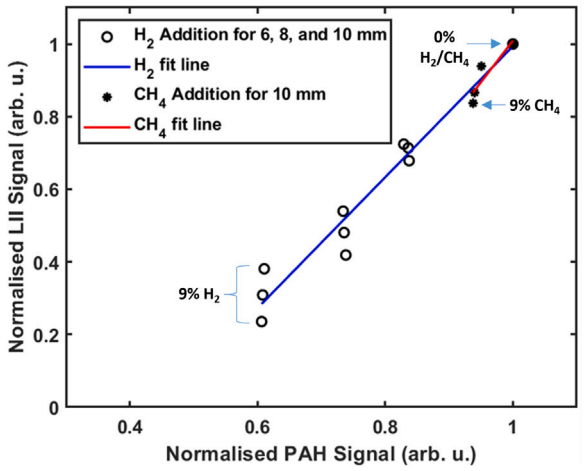

Fig. 8. The correlation between normalised peak signals of PAH LIF and LII in C_2H_4 flames enriched with H_2 and CH_4. The open black circles and black dots represent experimental data for H_2 and CH_4 addition levels in the range of $0 \leq H_2/CH_4 \leq 9$. The blue and red lines indicate linear fits for H_2 and CH_4 enriched flames respectively, where $R^2 = 0.993$ (H_2) and 0.82 (CH_4).

LIF and LII signals for CH_4 addition. This could be attributed to the difference in the chemical effects of H_2 and CH_4; while direct addition of H_2 makes it readily available to influence soot inception and growth, the C-H bond in CH_4 would need to be broken firstly to release the H-atom or H_2. Furthermore, H_2 addition reduces the carbon per unit mass available for PAH and soot formation, and growth in the binary fuel mixture (dilution effects) to a greater extent than the addition of an equivalent volumetric amount of CH_4. Furthermore, it can be seen from Fig. 8 that a linear correlation exists between PAH LIF and LII for both H_2 and CH_4 addition, covering all HABs investigated. These observations are consistent with the role of PAHs as precursors to soot formation, with the rate of soot inception having a non-linear dependence on PAH concentration and the rate of soot growth being dependent on concentration of PAHs and of other precursors, such as acetylene, whose abundance is also likely to be diminished by H_2 addition. The influence of CH_4 addition is far less pronounced than that of H_2 and the confidence in the linear fit shown in Fig. 8 is correspondingly lower. Nevertheless, the linear fits seem to overlap, which raises a question about the generality of the correlation for other additives, which may merit further investigation. It would also be interesting to explore whether the linear trend continues for even greater H_2 addition, to the point where the line might reach the x-axis: extrapolation would suggest that a PAH LIF signal of about 45% of the maximum would be a threshold at which the flame might be free of soot.

4. Conclusion

The effect of hydrogen addition on soot and PAH formation in ethylene inverse diffusion flame was studied using LII (demonstrated with a long-pulsed fibre laser) and PAH-PLIF. Methane was also separately added to the ethylene flame to study its effects in comparison with the hydrogen addition cases. Some specific conclusions on the effect of H_2 and CH_4 addition on PAH and LII from this work are:

- The peak signal for both PAH LIF and LII was observed to increase monotonically as the height above burner (HAB) increased from 6 mm to 10 mm which was attributed to the effect of increased residence time which allowed further growth of PAH and consequently soot particles. The PAH LIF signal and LII signal were observed to increase by a factor of 2.9 and 4.3 respectively between HAB of 6 mm and 10 mm.
- With H_2 addition, the magnitude of reduction in the peak PAH signal showed no variation with HAB while slight variation with HAB was observed in the peak LII signal. For all cases of H_2 addition, a higher magnitude of reduction was observed for the peak LII signal when compared to the peak PAH signal.
- Comparing the effects of H_2 addition with CH_4 addition indicated that for all cases investigated, H_2 addition showed higher reductions in PAH LIF and LII. This was attributed to the difference in the reactive behaviour of H_2 addition and CH_4 addition; while H_2, when added, is readily available to interact with the soot formation and growth process, the C-H bond in CH_4 needs to be broken to release the H-atom or H_2.

CRediT authorship contribution statement

Chinonso Ezenwajiaku: Writing – review & editing, Writing – original draft, Methodology, Investigation, Funding acquisition, Formal analysis, Conceptualization. **Robert Roy:** Methodology, Investigation, Formal analysis, Conceptualization. **Midhat Talibi:** Writing – review & editing, Supervision, Project administration, Methodology, Funding acquisition, Conceptualization. **Ramanarayanan Balachandran:** Writing – review & editing, Supervision, Project administration, Methodology, Funding acquisition, Conceptualization. **Iain S. Burns:** Writing – review & editing, Supervision, Project administration, Methodology, Funding acquisition, Conceptualization.

Declaration of competing interest

The authors declare that they have no known competing financial interests or personal relationships that could have appeared to influence the work reported in this paper.

Data availability

Data will be made available on request.

Acknowledgements

MT, RB and CE would like to acknowledge UKRI Future Leaders Fellowship (MR/T019735/1), UK Engineering and Physical Sciences Research Council (EPSRC) (EP/P003036/1) and the Nigerian Petroleum Technology Development Fund (PTDF) (PTDF/ED/PHD/ECE/97/16) for their financial support towards this work. IB and RR acknowledge financial support from EPSRC Platform Grant (EP/P001661/1) and from the European Union's Horizon 2020 Research and Innovation Framework Programme under grant agreement No 785539.

References

[1] Johansson K, Head-Gordon M, Schrader P, Wilson K, Michelsen H. Resonance-stabilized hydrocarbon-radical chain reactions may explain soot inception and growth. Science 2018;361(6406):997–1000.
[2] Niranjan R, Thakur AK. The toxicological mechanisms of environmental soot (black carbon) and carbon black: focus on oxidative stress and inflammatory pathways. Front. Immunol. 2017;8:763.
[3] Singh P, Hui X, Sung C-J. Soot formation in non-premixed counterflow flames of butane and butanol isomers. Combust Flame 2016;164:167–82.
[4] Humphries GS, Roy R, Black JD, Lengden M, Burns IS. In situ photoacoustic measurement of soot profiles in laminar flames using a high-repetition-rate pulsed fibre laser. Appl Phys B 2019;125:1–6.
[5] Blevins LG, Fletcher RA, Benner Jr BA, Steel EB, Mulholland GW. The existence of young soot in the exhaust of inverse diffusion flames. Proc. Combust. Inst. 2002;29(2):2325–33.
[6] Vander Wal RL. Soot precursor material: Visualization via simultaneous LIF-LII and characterization via TEM. In: Symposium (International) on Combustion. vol. 26, Elsevier; 1996, p. 2269–75, (2).
[7] Katta VR, Blevins LG, Roquemore WM. Dynamics of an inverse diffusion flame and its role in polycyclic-aromatic-hydrocarbon and soot formation. Combust Flame 2005;142(1–2):33–51.
[8] Santamaría A, Mondragón F, Molina A, Marsh ND, Eddings EG, Sarofim AF. FT-IR and 1H NMR characterization of the products of an ethylene inverse diffusion flame. Combust. Flame 2006;146(1–2):52–62.
[9] McEnally CS, Pfefferle LD. The effects of premixing on soot production in non-premixed flames fueled with unsaturated hydrocarbons. Proc. Combust. Inst. 2002;29(2):2407–13.
[10] Sidebotham GW, Glassman I. Flame temperature, fuel structure, and fuel concentration effects on soot formation in inverse diffusion flames. Combust. Flame 1992;90(3–4):269–83.
[11] Mikofski MA, Williams TC, Shaddix CR, Fernandez-Pello AC, Blevins LG. Structure of laminar sooting inverse diffusion flames. Combust. Flame 2007;149(4):463–78.
[12] Sun Z, Dally B, Nathan G, Alwahabi Z. Effects of hydrogen and nitrogen on soot volume fraction, primary particle diameter and temperature in laminar ethylene/air diffusion flames. Combust Flame 2017;175:270–82.
[13] Liu F, He X, Ma X, Zhang Q, Thomson M, Guo H, Smallwood G, Shuai S, Wang J. An experimental and numerical study of the effects of dimethyl ether addition to fuel on polycyclic aromatic hydrocarbon and soot formation in laminar coflow ethylene/air diffusion flames. Combust. Flame 2011;158(3):547–63.
[14] Karataş AE, Gülder ÖL. Dependence of sooting characteristics and temperature field of co-flow laminar pure and nitrogen-diluted ethylene–air diffusion flames on pressure. Combust Flame 2015;162(4):1566–74.
[15] Barak S, Rahman RK, Neupane S, Ninnemann E, Arafin F, Laich A, Terracciano AC, Vasu SS. Measuring the effectiveness of high-performance co-optima biofuels on suppressing soot formation at high temperature. Proc Natl Acad Sci 2020;117(7):3451–60.
[16] Desgroux P, Mercier X, Thomson KA. Study of the formation of soot and its precursors in flames using optical diagnostics. Proc. Combust. Inst. 2013;34(1):1713–38.
[17] Trottier S, Guo H, Smallwood G, Johnson M. Measurement and modeling of the sooting propensity of binary fuel mixtures. Proc. Combust. Inst. 2007;31(1):611–9.
[18] Tian B, Gao Y, Zhang C, Hochgreb S. Soot measurement in diluted methane diffusion flames by multi-pass extinction and laser-induced incandescence. Combust Flame 2018;192:224–37.
[19] Sun Z, Gu D, Nathan G, Alwahabi Z, Dally B. Single-shot, time-resolved planar laser-induced incandescence (TiRe-LII) for soot primary particle sizing in flames. Proc. Combust. Inst. 2015;35(3):3673–80.
[20] Conturso M, Sirignano M, D'Anna A. Effect of C_9H_{12} alkylbenzenes on particle formation in diffusion flames: An experimental study. Fuel 2017;191:204–11.
[21] Sirignano M, Ciajolo A, D'Anna A, Russo C. Particle formation in premixed ethylene-benzene flames: An experimental and modeling study. Combust Flame 2019;200:23–31.
[22] Liu F, Hua Y, Wu H, Lee C-f, He X. An experimental study on soot distribution characteristics of ethanol-gasoline blends in laminar diffusion flames. J. Energy Inst. 2018;91(6):997–1008.
[23] Atiku F, Lea-Langton A, Bartle K, Jones J, Williams A, Burns I, Humphries G. Some aspects of the mechanism of formation of smoke from the combustion of wood. Energy Fuels 2017;31(2):1935–44.
[24] Vander Wal R, Weiland K. Laser-induced incandescence: development and characterization towards a measurement of soot-volume fraction. Appl Phys B 1994;59:445–52.
[25] Jurng J. Experimental approaches of laser-induced incandescence technique for soot measurement. In: Technical Digest. CLEO/Pacific Rim'99. Pacific Rim Conference on Lasers and Electro-Optics (Cat. No. 99TH8464). vol. 2, IEEE; 1999, p. 161–2.
[26] Migliorini F, De Iuliis S, Dondè R, Commodo M, Minutolo P, D'Anna A. Nanosecond laser irradiation of soot particles: Insights on structure and optical properties. Exp Therm Fluid Sci 2020;114:110064.
[27] Bartos D, Sirignano M, Dunn MJ, D'Anna A, Masri AR. Soot inception in laminar coflow diffusion flames. Combust Flame 2019;205:180–92.
[28] Schulz C, Kock BF, Hofmann M, Michelsen H, Will S, Bougie B, Suntz R, Smallwood G. Laser-induced incandescence: recent trends and current questions. Appl Phys B 2006;83:333–54.
[29] Michelsen HA, Schulz C, Smallwood GJ, Will S. Laser-induced incandescence: Particulate diagnostics for combustion, atmospheric, and industrial applications. Prog Energy Combust Sci 2015;51:2–48.
[30] McCormick D, Ozanyan KB, Black JD, Feng Y. In-situ soot particle sensing in an aero-engine exhaust plume. In: Sensors, 2013 IEEE. IEEE; 2013, p. 1–4.
[31] McCormick D, Black JD, Feng Y, Nilsson J, Ozanyan KB. High-sensitivity in situ soot particle sensing in an aero-engine exhaust plume using long-pulsed fiber-laser-induced incandescence. IEEE Sens J 2015;16(8):2674–82.

[32] Black JD. Fiber lasers as a source for laser-induced incandescence in practical applications. In: Laser Applications To Chemical, Security and Environmental Analysis. Optica Publishing Group; 2010, p. LWB5.
[33] Roy RG. Laser induced incandescence imaging for the investigation of soot formation in laminar flames (Ph.D. thesis), University of Strathclyde; 2019.
[34] Liu F, Ai Y, Kong W. Effect of hydrogen and helium addition to fuel on soot formation in an axisymmetric coflow laminar methane/air diffusion flame. Int J Hydrogen Energy 2014;39(8):3936–46.
[35] Park S-H, Lee K-M, Hwang C-H. Effects of hydrogen addition on soot formation and oxidation in laminar premixed C_2H_2/air flames. Int J Hydrogen Energy 2011;36(15):9304–11.
[36] Gu M, Chu H, Liu F. Effects of simultaneous hydrogen enrichment and carbon dioxide dilution of fuel on soot formation in an axisymmetric coflow laminar ethylene/air diffusion flame. Combust Flame 2016;166:216–28.
[37] Xu L, Yan F, Wang Y, Chung SH. Chemical effects of hydrogen addition on soot formation in counterflow diffusion flames: Dependence on fuel type and oxidizer composition. Combust Flame 2020;213:14–25.
[38] De Iuliis S, Maffi S, Migliorini F, Cignoli F, Zizak G. Effect of hydrogen addition on soot formation in an ethylene/air premixed flame. Appl Phys B 2012;106(3):707–15.
[39] Yoon S, Lee S, Chung S. Effect of mixing methane, ethane, propane, and propene on the synergistic effect of PAH and soot formation in ethylene-base counterflow diffusion flames. Proc. Combust. Inst. 2005;30(1):1417–24.
[40] Roesler J, Martinot S, McEnally C, Pfefferle L, Delfau J-L, Vovelle C. Investigating the role of methane on the growth of aromatic hydrocarbons and soot in fundamental combustion processes. Combust. Flame 2003;134(3):249–60.
[41] Hwang J, Lee W, Kang H, Chung S. Synergistic effect of ethylene–propane mixture on soot formation in laminar diffusion flames. Combust. Flame 1998;114(3–4):370–80.
[42] Ni T, Gupta S, Santoro R. Suppression of soot formation in ethene laminar diffusion flames by chemical additives. In: Symposium (International) on Combustion. vol. 25, Elsevier; 1994, p. 585–92, (1).
[43] Ezenwajiaku C, Talibi M, Doan NAK, Swaminathan N, Balachandran R. Study of polycyclic aromatic hydrocarbons (PAH) in hydrogen-enriched methane diffusion flames. Int J Hydrogen Energy 2019;44(14):7642–55.
[44] Wu J, Song KH, Litzinger T, Lee S-Y, Santoro R, Linevsky M, Colket M, Liscinsky D. Reduction of PAH and soot in premixed ethylene–air flames by addition of ethanol. Combust. Flame 2006;144(4):675–87.
[45] Beretta F, Cincotti V, D'alessio A, Menna P. Ultraviolet and visible fluorescence in the fuel pyrolysis regions of gaseous diffusion flames. Combust. Flame 1985;61(3):211–8.
[46] Berlman I. Handbook of Florescence Spectra of Aromatic Molecules. London: Elsevier; 2012.
[47] Singh P, Sung C-J. PAH formation in counterflow non-premixed flames of butane and butanol isomers. Combust. Flame 2016;170:91–110.
[48] Mercier X, Carrivain O, Irimiea C, Faccinetto A, Therssen E. Dimers of polycyclic aromatic hydrocarbons: the missing pieces in the soot formation process. Phys Chem Chem Phys 2019;21(16):8282–94.
[49] Thomson MJ. Modeling soot formation in flames and reactors: Recent progress and current challenges. Proc. Combust. Inst. 2022.
[50] Ezenwajiaku C, Talibi M, Balachandran R. PAH formation characteristics in hydrogen-enriched non-premixed hydrocarbon flames. Fuel 2022;323:124407.
[51] Du D, Axelbaum R, Law CK. Soot formation in strained diffusion flames with gaseous additives. Combust. Flame 1995;102(1–2):11–20.
[52] Wang Y, Liu X, Gu M, An X. Numerical simulation of the effects of hydrogen addition to fuel on the structure and soot formation of a laminar axisymmetric coflow $C_2H_4/(O_2\text{-}CO_2)$ diffusion flame. Combust. Sci. Technol. 2018.
[53] Demarco R, Jerez A, Liu F, Chen L, Fuentes A. Modeling soot formation in laminar coflow ethylene inverse diffusion flames. Combust Flame 2021;232:111513.
[54] Khanehzar A, Cepeda F, Dworkin SB. The influence of nitrogen and hydrogen addition/dilution on soot formation in coflow ethylene/air diffusion flames. Fuel 2022;309:122244.